bioRχiv

PMP22 associates with MPZ via their transmembrane domains and disrupting this interaction causes a loss-of-function phenotype similar to hereditary neuropathy associated with liability to pressure palsies (HNPP).

Natalya Pashkova[1], Tabitha A. Peterson[1], Christopher P. Ptak[2], Stanley C. Winistorfer[1], Christopher A. Ahern[1], Michael E. Shy[1,3] and Robert C. Piper[1*]

1. Department of Molecular Physiology and Biophysics, Carver College of Medicine, University of Iowa, Iowa City 52242
2. Carver College of Medicine NMR facility, University of Iowa, Iowa City 52242
3. Department of Neurology, Carver College of Medicine, University of Iowa, Iowa City 52242

* robert-piper@uiowa.edu

PMP22 and MPZ are major myelin proteins in the peripheral nervous system. MPZ is a single pass integral membrane protein with an extracellular immunoglobulin (Ig)-like domain and works as an adhesion protein to hold myelin wraps together across the intraperiod line. Loss of MPZ causes severe demyelinating Charcot-Marie-Tooth (CMT) peripheral neuropathy. PMP22 is an integral membrane tetraspan protein belonging to the Claudin superfamily. Homozygous loss of PMP22 also leads to severe demyelinating neuropathy, and duplication of wildtype PMP22 causes the most common form of CMT, CMT1A. Yet the molecular functions provided by PMP22 and how its alteration causes CMT are unknown. Here we find that these abundant myelin proteins form a strong and specific complex. Mutagenesis and domain swapping experiments reveal that these proteins interact through interfaces within their transmembrane domains. We also find that the PMP22 A67T patient variant that causes an HNPP (Hereditary neuropathy with pressure palsies) phenotype, reflecting a heterozygous loss-of-function, maps to this interface. The PMP22 A67T variant results in the specific loss of MPZ association with PMP22 without affecting PMP22 localization to the plasma membrane or its interactions with other proteins. These data define the molecular basis for the MPZ~PMP22 interaction and indicate that the MPZ~PMP22 complex fulfills an important function in myelinating cells.

Introduction

Large diameter axons in the peripheral nervous system (PNS) are insulated by wraps of myelin sheath produced by Schwann cells to ensure rapid and efficient transmission of electrical impulses. Heritable neuropathies of the PNS are often referred to as Charcot Marie Tooth (CMT) disease. CMT is the most frequently diagnosed set of genetic neuromuscular diseases, affecting 1:2500 individuals (Skre, 1974). Autosomal dominant inheritance CMT is the most common, followed by X-linked and autosomal recessive forms. Most forms of CMT are demyelinating and characterized by poorly formed myelin (CMT1), whereas one-third of CMT cases are primary axonal disorders (CMT2) in which axons degenerate but myelin formation is relatively normal (Fridman et al., 2015; Murphy et al., 2012).

Two crucial Schwann cell proteins involved in the structure and function of myelin are Myelin Protein Zero (MPZ) and Peripheral Myelin Protein 22 (PMP22). Alteration of these proteins can cause CMT. MPZ comprises ~50% of myelin protein (Lemke and Axel, 1985; Uyemura et al., 1995), and is a single-pass transmembrane protein with a single immunoglobulin-like (Ig) extracellular domain and cytosolic tail (Eylar et al., 1979; Greenfield et al., 1973). It is post-translationally modified by N-linked glycosylation, sulfation, palmitoylation, and phosphorylation (D'Urso et al., 1990; Eichberg and Iyer, 1996). MPZ is an adhesion protein, holding together adjacent wraps of myelin membrane across the intraperiod line (Filbin et al., 1990; Giese et al., 1992; Xu et al., 2001). MPZ also uses its cytosolic tail to promote myelin compaction of the cytosolic region between myelin wraps to form the major dense line (Filbin et al., 1999; Mandich et al., 1999; Xu et al., 2001). Thus, MPZ resembles other adhesion molecules such as cadherins and integrins that couple their extracellular domains to the cytoskeleton as well as providing signaling cascades through their cytosolic domains. Variants in MPZ account for 5% of CMT cases overall and can cause demyelinating or axonal phenotypes, reflecting the diverse roles of MPZ in Schwann cells (Fridman et al., 2015; Fridman et al., 2023; Hayasaka et al., 1993).

PMP22 is also a major component of myelin. There have been many functions proposed for PMP22, yet the molecular and cellular functions of PMP22 used to promote normal myelination remain unclear (Fabbretti et al., 1995; Jetten and Suter, 2000; Lee et al., 2014; Lee et al., 2018; Notterpek et al., 2001; Vanoye et al., 2019; Zhou et al., 2020; Zhou et al., 2019; Zoidl et al., 1995). PMP22 is a glycosylated 4-pass integral membrane protein that belongs to a subfamily of claudin-related proteins that includes EMP1, EMP2, and EMP3 (Van Itallie and Anderson, 2006). An emerging view is that PMP22/EMP family proteins promote adhesion and interact with adhesion proteins (Ahmat Amin et al., 2019; Amici et al., 2006; Qin et al., 2015; Simske, 2013). Unlike MPZ, which is exclusively expressed in Schwann cells,

PMP22 shows a broader pattern of expression and has been found at tight junctions between epithelial cells suggesting it can help organize adhesion structures (Lemke and Axel, 1985; Notterpek et al., 2001; Roux et al., 2005). Moreover, PMP22 can help adhere membranes together in a variety of *in vitro* contexts (Hasse et al., 2004; Jung et al., 2011; Mittendorf et al., 2017). Consistent with a potential role in adhesion, PMP22 has been found to associate (directly or indirectly) with a variety of other proteins including Jam-C, integrins, myelin-associated glycoprotein (MAP) and oligomerization with PMP22 itself (Fantin et al., 2021; Guo et al., 2014; Rao et al., 2011; Tobler et al., 1999). Overall, alteration of PMP22 accounts for approximately 50% of CMT cases (Rossor et al., 2013; van Paassen et al., 2014). The majority of demyelinating cases of CMT (CMT1A) are caused by an extra copy of wildtype *PMP22* (Li et al., 2013; Lupski et al., 1992; Pantera et al., 2020; Timmerman et al., 1992). However, heterologous deletion of *PMP22* causes HNPP (Hereditary neuropathy with pressure palsies), a milder form of peripheral neuropathy reflecting a partial loss-of-function phenotype (Chance et al., 1993). These observations underscore the importance of having the critical balance of PMP22 levels for proper myelination. Most newly synthesized PMP22 is degraded in Schwann cells (Pareek et al., 1997), and part of how overexpression or variants of PMP22 cause CMT may be due to Endoplasmic Reticulum (ER) stress (Colby et al., 2000; Hara et al., 2014; Lupski et al., 1992; Marinko et al., 2020a; Pantera et al., 2020), exacerbated by the ability of PMP22 to alter ER membrane morphology (Mittendorf et al., 2017). However, whether that serves as the primary mechanism for CMT pathogenesis or whether PMP22 works in conjunction with other proteins to cause CMT is not clear.

We found that MPZ forms a strong and specific complex with PMP22. Though previous studies suggested MPZ forms a complex with PMP22 (D'Urso et al., 1999; Hasse et al., 2004), the biochemical basis and specificity of that interaction were not defined nor validated by others. Our data demonstrate a robust and specific interaction of MPZ and PMP22 mediated by their transmembrane domains (TMD). Within these interacting interfaces lies the patient variant A67T, which causes an HNPP phenotype, reflecting a PMP22 heterozygous loss-of-function. We find that the A67T variant disrupts MPZ~PMP22 complex without affecting PMP22 localization to the plasma membrane nor association with other PMP22-interacting proteins. These data suggest the interaction between MPZ and PMP22 serves a critical function in myelin.

Results

MPZ forms a complex with PMP22

We found that PMP22 forms a very specific and strong interaction with MPZ in HEK293 cells and rat RT4 Schwannoma cells. Figure 1 shows that PMP22-GFP co-immunoprecipitates with C-terminally HA-tagged MPZ when both are co-expressed in HEK293 cells (Figure 1A) and RT4 Schwannoma cells (Figure 1C). However, no complex was found between MPZ and the PMP22-related protein EMP3 (Figure 1C). Immunoprecipitations were accomplished using Sepharose coupled to α-GFP nanobodies. In general, these observations partly align with previous studies showing evidence that PMP22 and MPZ form a complex (D'Urso et al., 1999; Hasse et al., 2004). We found non-ionic detergents destroyed the complex whereas a detergent formulation of DDM (n-dodecyl-β-d-maltoside) and CHS (cholesterol-like cholesteryl hemisuccinate) preserved the complex (Figure 1A). Previous studies used a mix of non-ionic detergents within their lysis buffer (D'Urso et al., 1999). However, biological membranes contain zwitterionic and negatively charged head groups that can affect membrane protein interactions and functions, which could be disrupted by detergents such as those previously used (e.g. NP40 and Triton X-100). In contrast, amphipathic environments can be maintained by using DDM and CHS detergents. Previous studies indicate that PMP22 is cholesterol-phillic (Castello-Serrano et al., 2020; Hasse et al., 2002; Marinko et al., 2020b; Zhou et al., 2020; Zhou et al., 2019) and that higher-order oligomers of PMP22 *in vitro* appear to be preserved using cholesterol-like environments (Fantin et al., 2021). These biophysical properties provide a foundation to study the MPZ~PMP22 complex and provide an explanation for why detection of this complex may have been difficult for other investigators.

To investigate protein interactions, we used GFP-tagged PMP22 where GFP was fused to the PMP22 C-terminus. Previous studies found that GFP fusion to PMP22 had the potential to drive aggregation (D'Urso et al., 1998; Dickson et al., 2002; Liu et al., 2004), which could confound our co-immunoprecipitation experiments. We sought to circumvent this problem by using monomeric superfolder GFP (msGFP2) (Valbuena et al., 2020) separated by a short flexible linker. As tested by size exclusion chromatography, DDM/CHS-solubilized PMP22-GFP eluted as a major peak at ~120kDa which is consistent with a PMP22-GFP dimer. No significant proportion of heterogeneous GFP-fusion aggregates were found in the void volume resolved by Superose 6 column (*Supplemental Figure 1*). To confirm the MPZ-PMP22 interaction, we also used a PMP22 carrying a myc tag inserted into its second extracellular loop, previously reported to provide an epitope-tagged form of PMP22 that is not prone to aggregation (Liu et al., 2004). Figure 1D shows that PMP22-myc^{exo} also efficiently co-immunoprecipitated with MPZ-GFP.

We next sought to determine whether the PMP22~MPZ complex can only be formed by proteins expressed together in the same cells. Figure 1B shows that when MPZ-HA and PMP22-GFP are co-expressed in the same cell (labeled as 'pre'), they can efficiently be co-immunoprecipitated. However, when expressed in separate cell populations and mixed after lysis (labeled as 'post'), the PMP22~MPZ complex could not be recovered by co-immunoprecipitation. In all experiments, we found that a large proportion of MPZ-HA was recovered in a complex with co-immunoprecipitated PMP22-GFP as judged by the ratio to the levels of MPZ-HA present in the input lysate. These results indicate that the association of MPZ with PMP22 is

strong, efficient, and may be near stoichiometric. We also found that MPZ-HA forms a complex with MPZ-GFP when expressed in the same cell, consistent with its ability to oligomerize (Ptak et al., 2023; Sakakura et al., 2011; Shapiro et al., 1996). In contrast, however, the efficiency of MPZ~MPZ complex recovery was far less than that of the PMP22~MPZ complex recovery (Figure 1B).

In addition, we confirmed that PMP22-GFP associated with MPZ-mCherry within the plasma membrane of HEK293 cells as assessed by FRET measured by donor fluorescence-enhancement after acceptor photobleaching (Figure 1E). MPZ tandemly fused to both msGFP2 and mCherry was used as a positive control which gave a percent FRET efficiency of 23.7%. As a negative control we used MPZ-mCherry co-expressed with glycophorin A-GFP, both of which localize to the plasma membrane but are not known to interact. The combination of MPZ-mCherry with PMP22-GFP had a FRET efficiency significantly different than the negative control pair (7.9%±4.2 vs 1.4%±2.0, respectively). Co-expressed MPZ-mCherry and MPZ-GFP also had a significant FRET efficiency above the negative control (5.3%±2.9 vs 1.4%±2.0, respectively). Most ROIs used for FRET measurements were areas of the plasma membrane that were not juxtaposed to other cell plasma membranes. For the few ROIs that we sampled on the plasma membrane areas between 2 cells, we saw no increased FRET efficiency, all of which indicated that the FRET signal we observed was from proteins interacting within the same bilayer in *cis*.

Specificity of the MPZ~PMP22 association.

Both MPZ and PMP22 each belong to subfamilies of homologous proteins. We found MPZ is the only member of its subfamily to interact with PMP22, and PMP22 is the only member of its subfamily to interact with MPZ. MPZ belongs to a subfamily of single-pass transmembrane proteins that contain an extracellular Ig-like domain that includes MPZL1, MPZL2, and subunits of voltage-gated sodium channels (SCN2B, SCN3B, and SCN4B) (Molinarolo et al., 2018). Figure 2A shows that PMP22 strongly co-immunoprecipitated with MPZ-HA, very weakly with MPZL2, and showed no co-immunoprecipitation with other MPZ family members MPZL1, SCN2B, SCN3B, or SCN4B. In contrast, while the PMP22 related protein EMP3 did not interact with MPZ-HA, it did interact strongly with MPZL2, SCN2B and SCN3B and also had a weak interaction with MPZL1.

We next exploited this specificity to map the regions necessary and sufficient for PMP22~MPZ interaction using a set of chimeric MPZ/β-subunit proteins where the extracellular Ig-like domain, transmembrane domains, and cytosolic tails were swapped. The exact composition of these chimeric proteins is provided in supplementary materials and provided schematically in Figure 2B. Chimeras made of parts of MPZL1 and SCN2B that contained the MPZ TMD were all able to form a complex with PMP22-GFP as assessed

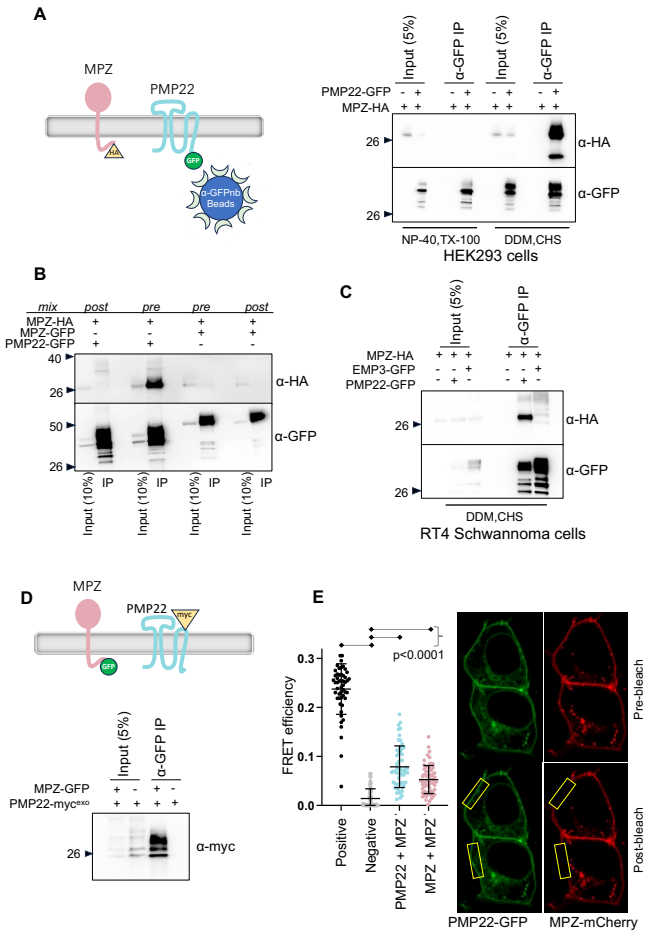

Figure 1: MPZ and PMP22 form a complex in HEK293 and RT4 Schwannoma cells. **A**. Left panel shows scheme for co-immunoprecipitation in which MPZ carrying a C-terminal HA eiptope tag and PMP22 carrying a C-terminal GFP tag are co-expressed and then immunoprecipitated with Sepharose linked to α-GFP nanobodies. Right panel shows results of co-immunoprecipitation. Lysates from HEK293 cells transiently co-transfected with MPZ-HA and PMP22-GFP were prepared with 0.5% NP-40 and 0.5% Triton X-100 or with 1% DDM and 0.2% CHS detergents. Bead-bound precipitates were washed in PBS with their respective detergents and eluted with SDS sample buffer. A proportion of the input (5%) was analyzed along with precipitated complexes by SDS-PAGE and immunoblotting with mouse α-HA (to detect associated MPZ-HA) and mouse α-GFP (to show efficiency of PMP22-GFP immunoprecipitation).
B. The co-immunoprecipitation scheme in A was used for HEK293 cells in which PMP22-GFP and MPZ-HA were co-expressed together before (pre) lysis or were expressed in separate populations and mixed after lysis (post). Co-immunoprecipitation was measured between PMP22-GFP and MPZ-HA or MPZ-GFP and MPZ-HA. Immunoprecipitates together with a 10% equivalent of the starting input was immunoblotted with anti-HA to reveal associated MPZ-HA. Note that while MPZ-HA associates with MPZ-GFP, the level of this association is far less than that with PMP22-GFP. Moreover, both associations required that proteins had to be expressed in the same cells prior to detergent lysis to detect the presence of MPZ~MPZ or MPZ~PMP22 complexes.
C. Co-immunoprecipitation of PMP22-GFP and MPZ-HA from DDM/CHS detergent lysates of transiently transfected RT4 Schwannoma cells. Whereas MPZ-HA was co-precipitated with PMP22-GFP, it was not co-precipitated with the PMP22-related protein EMP3-GFP.
D. Top panel shows scheme for co-immunoprecipitation of MPZ-GFP with PMP22 containing an exofacial myc epitope tag inserted into the second extracellular loop. Bottom panel shows PMP22-myc^{exo} is recovered when co-expressed with MPZ-GFP and immunoprecipitated with α-GFP nanobody beads.
E. Quantitation of FRET efficiency between PMP22-GFP and MPZ-mCherry and between MPZ-GFP and MPZ-mCherry. FRET was measured as an increase in donor fluorescence after acceptor photobleaching in transiently transfected HEK293 cells. The 'positive' control was MPZ tandemly fused to both msGFP2 and mCherry. The 'negative' control was Glycophorin A-GFP and MPZ-mCherry. Regions of interest were analyzed and quantified for at least 25 cells from 2 different experiments. FRET efficiencies were calculated with the Leica LAS X Microlab module. All ROI data are represented singly and aggregated as mean FRET efficiency ± S.D (from left to right 0.237±0.052, 0.014±0.020, 0.079±0.042, 0.053±0.029). One-way Anova with Turkey's multiple comparison test revealed the negative control was significantly different to each of the other samples. On the right is a representative FRET image of PMP22-GFP + MPZ-mCherry. The yellow boxes on the images show regions of interest used for bleaching and FRET measurements.

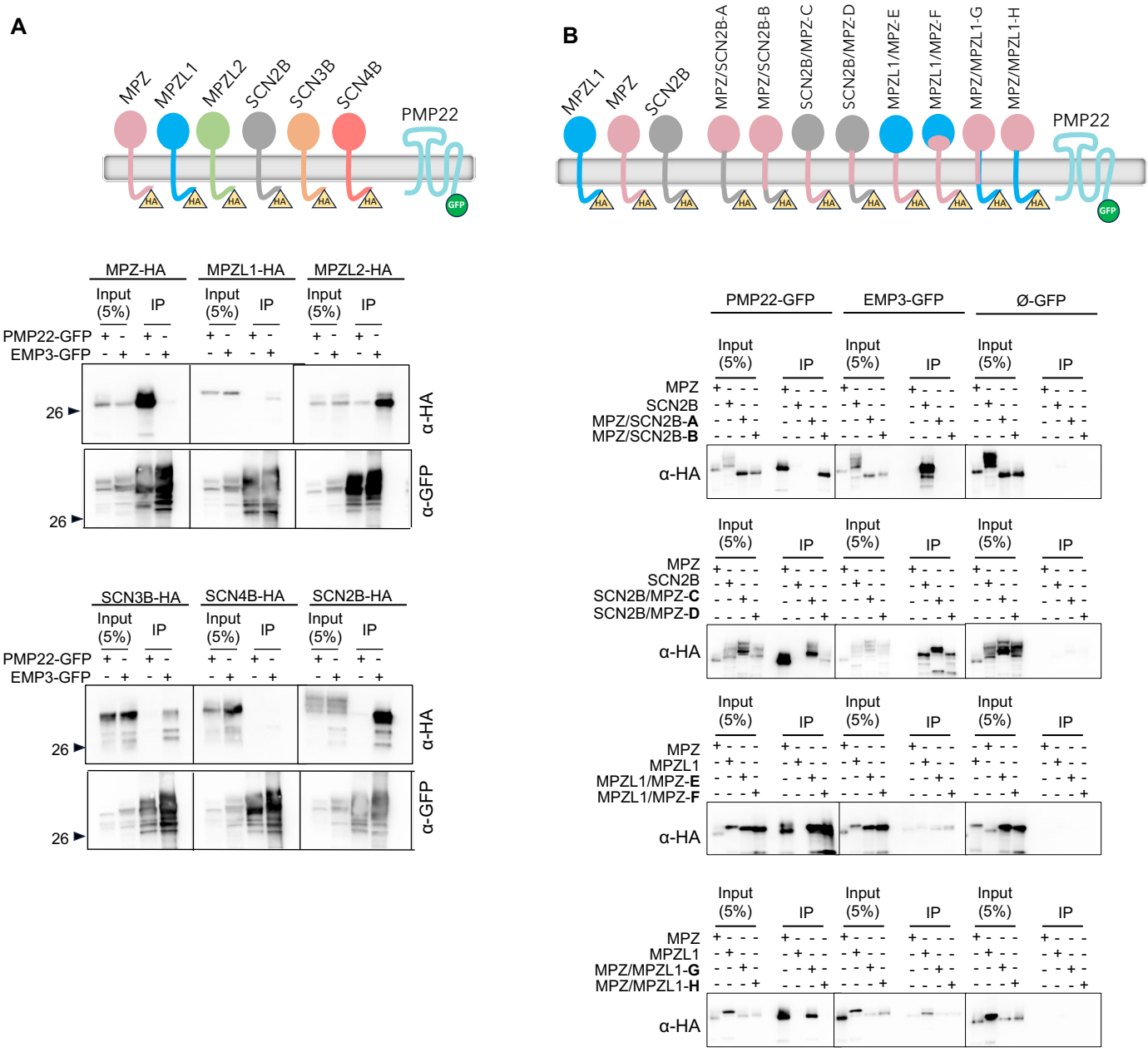

Figure 2. Specificity of MPZ association with PMP22 **A**. Several members of the MPZ/β-subunit family were assessed for their ability to associate with PMP22-GFP using the co-immunoprecipitation scheme outlined in Figure 1. DDM/CHS detergent lysates from HEK293 cells expressing the indicated HA-tagged MPZ/β-subunit proteins with either PMP22-GFP or EMP3-GFP were immunoprecipitated with α-GFP nanobody beads. Immunoprecipitation of PMP22-GFP only efficiently recovered MPZ-HA and a very low level of MPZL1. In contrast, MPZL2, SCN3B, and SCN2B formed strong complexes with EMP3-GFP. A 5% equivalent of the input lysate was included in each immunoblot.
B. The indicated HA-epitope tagged chimeric proteins made of the extracellular Ig-like domain, TMD, and cytosolic domains of MPZL1, SCN2B, and MPZ were assessed for association with PMP22-GFP, EMP3-GFP, or GFP alone (Ø-GFP) as described in A. Chimeras containing the TMD of MPZ were all co-precipitated with PMP22-GFP whereas substitution of the extracellular domain or cytosolic domain of MPZ with that of SCN2B or MPZL1 did not block PMP22 association. In contrast, the ability of SCN2B to associate with EMP3-GFP is conferred by its extracellular Ig-like containing domain.

by co-immunoprecipitation. These include chimeras B, C, and D (containing the MPZ TMD within the context of SCN2B) and chimeras E, F and G (containing the MPZ TMD within the context of MPZL1). We also examined whether these chimeras were informative about the regions that mediate association of EMP3 with SCN2B. Here, the data indicated that the extracellular Ig-like domain-containing region of SCB2B was necessary and sufficient for interaction with EMP3. Together, these data emphasize the specificity that PMP22 has for associating with MPZ over other MPZ/β-subunit family members and demonstrate that association is mediated through the MPZ TMD. These data also show that association of other MPZ/β-subunit members with different PMP22 family members (eg SCN2B association with EMP3) is not exclusively through transmembrane regions.

PMP22 Interaction surface on the transmembrane domain of MPZ.

We next determined which amino acids within the MPZ TMD were critical for PMP22 association. Because TMD interactions are mediated primarily via shape complementarity (Fink et al., 2012), we altered large bulky hydrophobic residues to small ones (eg. I/L to A) and *vice versa*. These mutations were made in the context of MPZ-mCherry to allow the subcellular localization of each mutant to be easily followed by microscopy to ensure that loss of

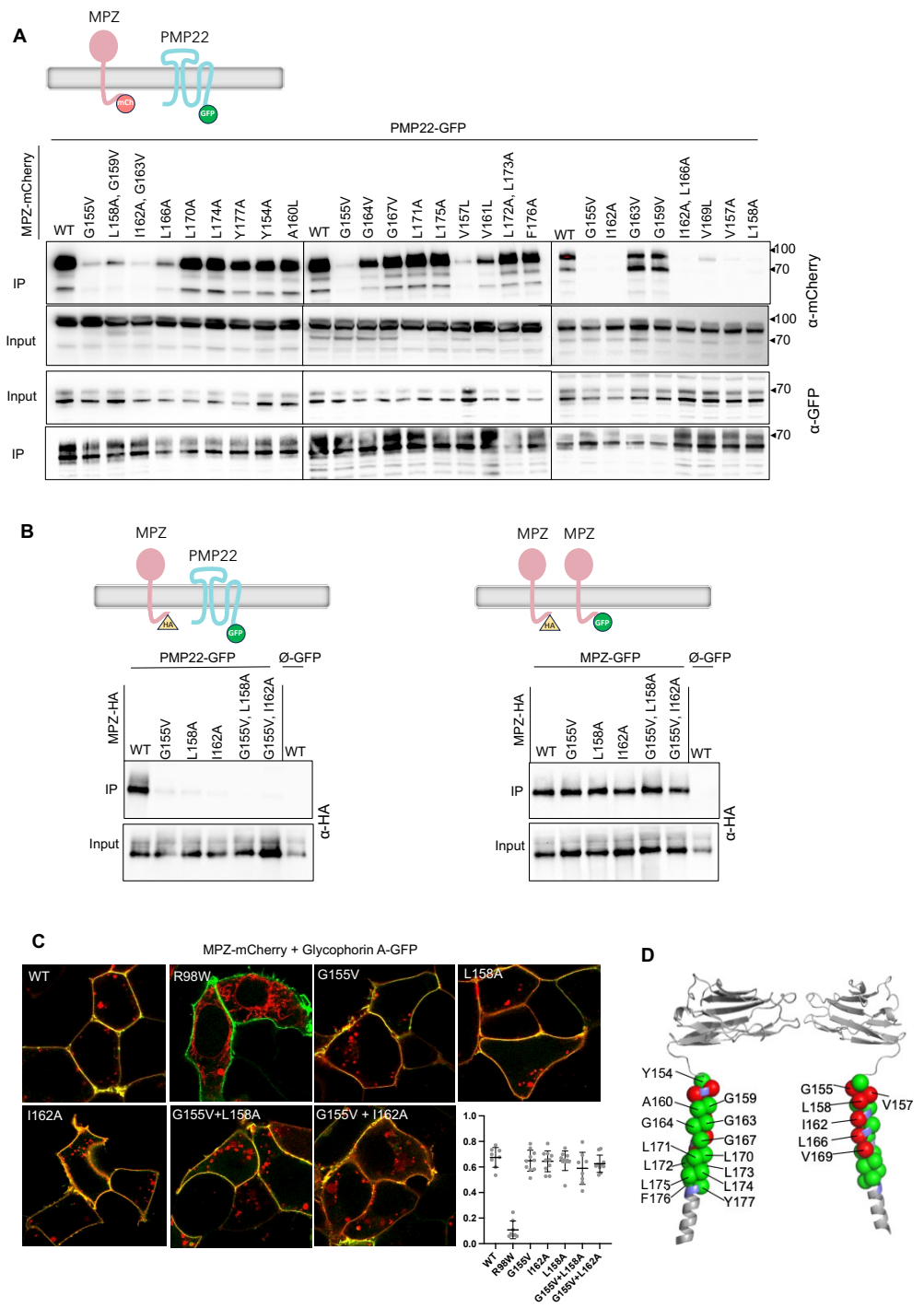

Figure 3. Mapping the PMP22-interacting interface within the MPZ transmembrane segment.

A. Top panel shows experimental scheme in which PMP22-GFP is co-expressed with mutant versions of MPZ-mCherry and immunoprecipitated with α-GFP nanobody beads. Lower panel shows immunoprecipitation results on the indicated MPZ-mCherry mutants.

B. Left. Results from A were verified using MPZ mutants in the context of a MPZ C-terminally HA-epitope-tagged protein co-expressed with PMP22-GFP or GFP alone (Ø-GFP) by coimmunoprecipitation with α-GFP nanobody beads and immunoblotting with α-HA antibodies. Right. WT and the indicated MPZ-HA mutants were assessed for their ability to oligomerize with MPZ-GFP using α-GFP nanobody beads.

C. Cell surface localization of WT MPZ-mCherry and the indicated mutants was assessed by confocal microscopy. Micrographs show WT MPZ-mCherry at the plasma membrane marked by Glycophorin A tagged with GFP, and puncta likely corresponding to endosomes. The MPZ R98W mutant, which is known to be retained in the ER, was included for comparison. Multiple fields encompassing >100 cells were assessed for overlap of MPZ-mCherry with the plasma membrane marker Glycophorin A using Manders overlap coefficient and plotted for each field in graph at right along with mean +SD. One way ANOVA revealed no differences in cell surface localization ($p>0.1$) amongst mutants and the WT MPZ-mCherry with the exception of the R98W mutant that had a significantly lower cell surface localization ($p<0.0001$) to every other MPZ-mCherry protein analyzed.

D. Residues in the MPZ TMD that when mutated had no effect (green) and dramatic reduction (red) in the ability to associate with PMP22 were mapped onto a model (AlphaFold: AF-P25189-F1) of a portion of MPZ containing the extracellular Ig-like domain and the α-helical region encompassing the TMD. Note that the red residues align along one face of the α-helix forming a cluster indicating the likely interface mediating PMP22 association.

PMP22 interaction was not due to severe misfolding as would be indicated by retention in the ER. Each MPZ-mCherry mutant was co-expressed with PMP22-GFP and tested for association by co-immunoprecipitation with α-GFP nanobody beads. Figure 3A shows that mutations in a subset of MPZ TMD residues disrupted association with PMP22. These residues largely clustered on one face of the predicted transmembrane α-helix and located on the half of the TMD closest to the extracellular side of the membrane (Figure 3D). This cluster contains residues G155, L158, and L162, that we further confirmed as critical for interaction in the context of an C-terminal HA epitope-tagged MPZ (Figure 3B). We also found that neither these mutations singly or in combination had deleterious effects on the ability of MPZ-mCherry to traffic to the plasma membrane (Figure 3C) nor the ability to form an oligomeric complex with MPZ-GFP (Figure 3B and *Supplemental Figure 2*). Together, these data confirm that the interaction with PMP22 is conferred through the MPZ TMD and highlight a discrete region within this region that is likely to comprise the binding interface. In addition, these data provide well-characterized mutant versions of MPZ for *in vitro* and *in vivo* functional studies that have specifically lost their ability to associate with PMP22 but retain other protein interactions as well as correct trafficking to the cell surface.

Basis for how PMP22 interacts with MPZ.

Figure 4 shows that amongst the PMP22/EMP family of proteins, only PMP22 formed a complex with MPZ whereas GFP-tagged EMP1, EMP2 or EMP3 did not. To find regions of PMP22 that contribute to MPZ association, we initially made a set of chimeric proteins between PMP22 and EMP3 for co-immunoprecipitation

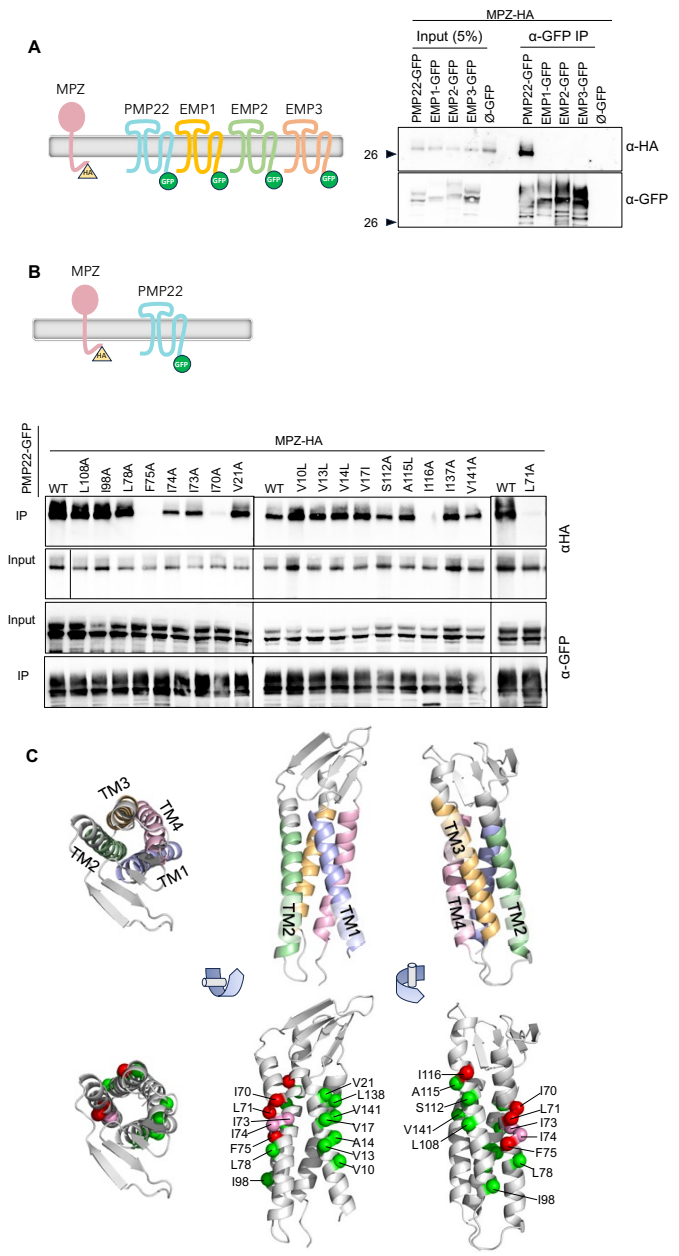

Figure 4. Specificity of PMP22 interaction with MPZ.
A. PMP22-GFP or the PMP22-related proteins EMP1-GFP, EMP2-GFP, EMP3-GFP, or GFP alone (Ø-GFP) were co-expressed with MPZ-HA in HEK293 cells and immunoprecipitated with α-GFP nanobodies. Immunoprecipitated eluted proteins were immunoblotted with α-HA to detect associated MPZ-HA and α-GFP to monitor recovery of PMP22-GFP. A 5% equivalent of the input lysate was included in the immunoblots.
B. The indicated amino acid substitutions were incorporated into PMP22-GFP and assessed for association with co-expressed MPZ-HA.
C. Model of PMP22 (AlphaFold: AF-Q01453-F1) showing orientation of the four transmembrne helices (TM1-4) of PMP22 and the predicted position of the amino acids critical for MPZ binding. Residues in PMP22 that when mutated had no effect (green), a partial reduction (pink) and dramatic reduction (red) in the ability to associate with MPZ are shown.

experiments. However, this approach was uninformative as chimeras containing swaps of 1 to 3 different transmembrane helices or extracellular loops largely compromised the ability of these chimeric proteins to associate with MPZ and did not yield a clear pattern for what region was required for association. Based on the data in Figure 3 indicating that residues residing in one half of the MPZ TMD were important for PMP22 association, we next focused on amino acid substitutions within the PMP22 transmembrane domains concentrating on residues within the four membrane-spanning helices closest to the extracellular side. Rather than use patient variants, we systematically analyzed each transmembrane helix by altering large hydrophobic residues to small ones (and *vice versa*) and assessing the impact on co-immunoprecipitation of these mutant PMP22 proteins with MPZ (Figure 4B). To rationalize this mutagenesis strategy, we mapped these mutation positions onto a previously determined homology model for PMP22 that was made based on its similarity to claudin-15 (PDB:4P79) for which a crystal structure is known (Mittendorf et al., 2014; Suzuki et al., 2014). We also used a model of PMP22 generated by Alphafold (Jumper et al., 2021), which predicted a structure very similar to claudin-15 and the previously determined PMP22 homology model (RMSD 0.98 and 1.311, respectively). Importantly, both models were highly similar within the membrane spanning segments (RMSD 0.95), bolstering the prediction of which residues were likely facing out of the TMD helical bundle and positioned for potential interactions with another protein *vs* those residues with side chains making intramolecular interactions between transmembrane helices that would likely be critical for the integrity of the PMP22 structure. Accordingly, we focused our mutagenesis on residues predicted to face outwardly. Several amino acid substitution mutations in PMP22 were found to ablate or dramatically reduce interaction with MPZ (Figure 4B,C). These include the I70A, L71A, F75A that map to a cluster of residues on one face of the 2nd transmembrane helix of PMP22 and which blocked MPZ association altogether. Altering residues near this cluster (e.g. I73A and I74A) but on a different face of the 2nd transmembrane helix diminished but did not destroy interaction with PMP22. Alteration of other residues along the 2nd transmembrane helix of PMP22 more toward the cytosolic side did not affect MPZ association. Similarly, amino acid substitutions within the 1st, 3rd, and 4th transmembrane helices of PMP22 were without effect on MPZ association with the exception of I116A near the extracellular edge on the third transmembrane helix.

The positions of the point mutants that disrupted the interaction between MPZ and PMP22 were used as restraints to generate a docking model to describe how MPZ might form a complex with PMP22 (Figure 5). Here, residues on one face of the 2nd transmembrane helix of PMP22 (I70, L71, and F75) are docked to residues on one face of the MPZ TMD (G155, L158, I162, and L166). It is not apparent in this model for how alteration of residue I116 to Alanine on the 3rd transmembrane helix of PMP22 blocks association with MPZ since I116 does not interact directly with MPZ. In Alphafold models of PMP22, I116 is packed against 2nd transmembrane helix (< 3 Å to W61, V65; < 4 Å to S64, T68; < 5 Å to L62) and the I116A mutation leads to a 43% reduction in residue-residue van der Waals contacts between the juxta-extracellular halves of the 2nd and 3rd transmembrane helices as assessed on the RING webserver (Clementel et al., 2022). The position of I116 suggests that a mutation may act indirectly by introducing structural or

dynamic changes that alter the ability of the 2nd PMP22 transmembrane helix to bind MPZ. Alternative models that include I116 as a docking restraint (shown in *Supplementary Figure 3*) reduced interactions for a number of residues that we found important for binding in mutagenesis experiments and also produced correspondingly higher restraint violation energies. These docking models are speculative and rely on the accuracy of the predicted structures for the individual interacting partners. Nonetheless, the models are instructive for highlighting potential interacting surfaces within the TMDs of PMP22 and MPZ that our mutagenesis and co-immunoprecipitation experiments define.

The interaction of PMP22 with MPZ is important for PMP22 function.

We next surveyed whether known PMP22 amino acid substitution patient variants that cause a range of peripheral neuropathy phenotypes had an impact on complex formation with MPZ. We focused on residues predicted to be on the outer facing surfaces of the TMDs and excluded residues that would potentially mediate intramolecular interactions between transmembrane helices and thus may be critical for proper PMP22 folding (Mittendorf et al., 2014). The A67T patient variant is located in the 2nd transmembrane helix in the midst of the cluster or residues we found by mutagenesis to be important for MPZ association (Figure 5A, B). Figure 5C shows that this patient variant dramatically blocked association with MPZ-HA as assessed by co-immunoprecipitation. In contrast, other PMP22 patient variants that are predicted to map to outwardly oriented residues of had no effect on MPZ association. These included A115V and T118M in the 3rd transmembrane helix and I137V in the 4th PMP22 transmembrane helix. The A67T variant was described in a patient with an HNPP phenotype, reflecting a heterozygous PMP22 loss-of-function (Nodera et al., 2003). This indicates that the association of PMP22 with MPZ may be a critical requirement for PMP22 to fully function in vivo.

Previous experiments have indicated that several biophysical properties as well as trafficking efficiency to the cell surface is largely preserved in the PMP22 A67T patient variant compared to WT PMP22 (Marinko et al., 2020b; Marinko et al., 2021; Schlebach et al., 2015). These observations support the idea that the loss of function for the A67T variant is specifically due to loss of MPZ association rather than an indirect effect due to perturbation of other properties. To test this idea further, we assessed whether PMP22 A67T preserved its ability to interact with other proteins (Figure 6). PMP22 has been found to form a complex with itself and with the double Ig-domain containing adhesion protein Jam-C (Guo et al., 2014; Schlebach et al., 2013; Tobler et al., 1999). In addition, during the course of our experiments, we discovered that PMP22 also interacts with the Jam-B adhesion protein and the PMP22-related protein, EMP1. Therefore, we determined whether the A67T patient variant as well as other amino acid substitutions within the presumed interface of PMP22 that mediates MPZ association preserved

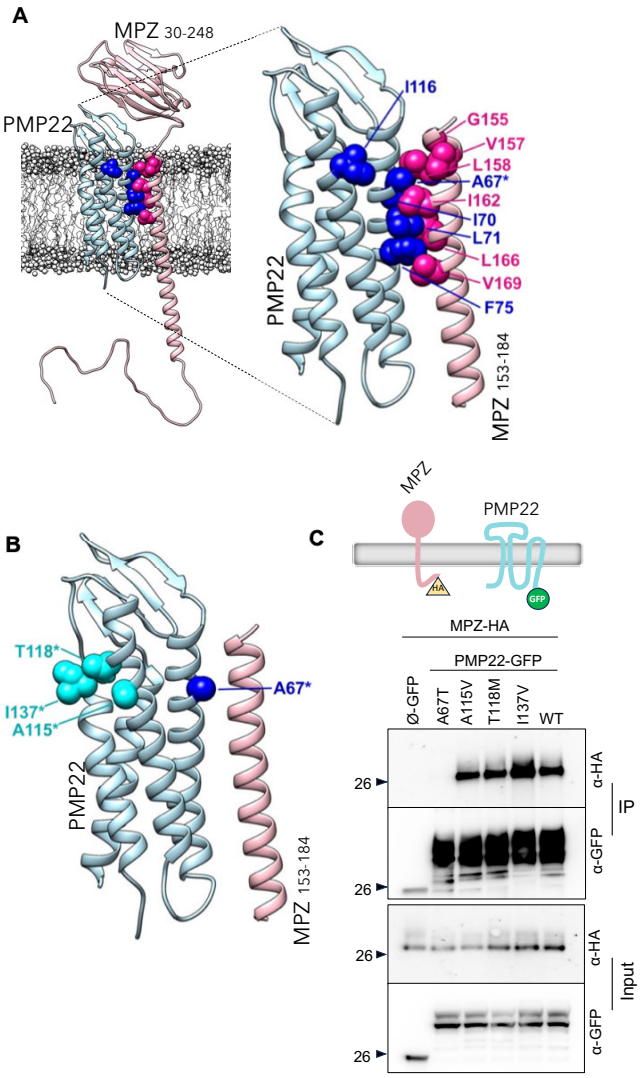

Figure 5. The patient variant of PMP22 (A67T) causing an HNPP phenotype maps to the presumed interface between PMP22 and MPZ.
A. Model of the complex between PMP22 and MPZ in which association is mediated by residues identified in amino acid substitution experiments. (Upper panel) The multi-component model composed of the full-length human PMP22 (light blue – AlphaFold: AF-Q01453-F1) and MPZ (pink – AlphaFold: AF-P25189-F1) is oriented in a lipid bilayer of 60% POPC : 40% cholesterol (white). For a few unstructured residues between MPZ domains, torsion adjustments were made for improved visualization of the extracellular domain and the flexible portion of the cytosolic tail. The residues that destroy or diminish the association of PMP22 and MPZ when mutated are indicated. The position of the HNPP-causing patient variant, A67T, which lies within the predicted interface mediating MPZ~PMP22 binding is indicated (*).
B. Model of the PMP22~MPZ interface shown in A with the positions of select patient variants including the A67T indicated on the different transmembranehelices
C. Effect of PMP22 patient variants on the association with MPZ. MPZ-HA was co-expressed with GFP alone (Ø-GFP), WT PMP22-GFP or the indicated PMP22 mutants and assessed for complex assembly by coimmunoprecipitation with α-GFP nanobody beads and immunoblotting for MPZ-HA with α-HA antibodies. Comparable expression levels of the different PMP22 mutants as well as the efficiency was assessed by immunoblotting input lysates and bead immunoprecipitates with α-GFP antibodies.

these protein interactions. Figure 6A shows that the PMP22-GFP carrying the A67T substitution or the I70A, I74A, or F75A were able to oligomerize with PMP22-HA and EMP1-HA as determined by co-immunoprecipitation. Likewise, these PMP22 mutants were also able to co-immunoprecipitate with both Jam-C-HA or Jam-B-HA, demonstrating that other protein interactions are unperturbed by these amino acid substitution mutations and indicate the overall integrity of the PMP22 structure remains intact.

We also measured how well each PMP22 mutant trafficked to the cell surface using a modified assay previously described that follows the exposure of a myc epitope tag when PMP22-myc^{exo} is localized to the cell surface (Marinko et al., 2020a). Here, PMP22-myc^{exo} is co-expressed on the same mRNA with a modified blue-fluorescent protein localized to the nucleus, a fiduciary signal to monitor the levels of PMP22-myc^{exo} production (Figure 6C). As a comparison, we also measured the trafficking efficiency of PMP22 G150D, the variant found in Trembler(Tr) mice known to trap PMP22 within the ER (Tobler et al., 2002). We found that PMP22-myc^{exo} carrying the A67T patient variant causing an HNPP phenotype was trafficked to the cell surface to the same extent as wildtype PMP22. Moreover, the amino acid substitutions within the 2nd transmembrane helix we found via systematic mutagenesis (eg. I70A, L71A, and F75A) also retained their ability to traffic to the cell surface. In contrast, PMP22 with the Trembler G150D mutation had a far lower efficiency of delivery to the cell surface and was found abundantly in the ER when cells were permeabilized before immunolabeling (*Supplemental Figure 4*).

Discussion

Here we find that two major myelin proteins, PMP22 and MPZ, form a strong and specific complex that is mediated by interactions between their transmembrane domains. That PMP22 and MPZ can form a complex has been previously proposed along with the model that their interaction is mediated by interactions between the extracellular domains potentially working in *trans* to bridge myelin wraps (D'Urso et al., 1990; D'Urso et al., 1999; Hasse et al., 2004). Those studies report using the non-ionic detergents NP-40 and Triton X-100 with which we were unable to recover any associated MPZ in PMP22 co-immunoprecipitates. Rather the integrity of the complex was preserved using DDM and CHS in which MPZ very efficiently associated with PMP22. Despite the paucity of insight into PMP22 function and the potential importance of the PMP22~MPZ complex, analysis of a PMP22~MPZ complex has not been pursued by other groups in the intervening 2 decades. We suggest that the remarkable dependence on proper detergent conditions described here for the preservation of the PMP22~MPZ complex may have been an impediment for further study. Previous data also indicated that MPZ may form its interaction with PMP22 *via* its extracellular Ig-like domain. However, these studies relied on interactions with a recombinant GST-MPZ-Ig fusion protein produced intracellularly in bacteria. The MPZ Ig-like domain maintains its structure via an intradomain disulfide bond which is perturbed in the reduced bacterial cytoplasmic environment, leading to production of a mis-folded aggregate (Sakakura et al., 2023). Similarly, we found that intracellularly produced recombinant MPZ Ig-like domain fused to GST, that itself contains a reactive cysteine, also produces a misfolded aggregate. Together, these data undermine the view that extracellular

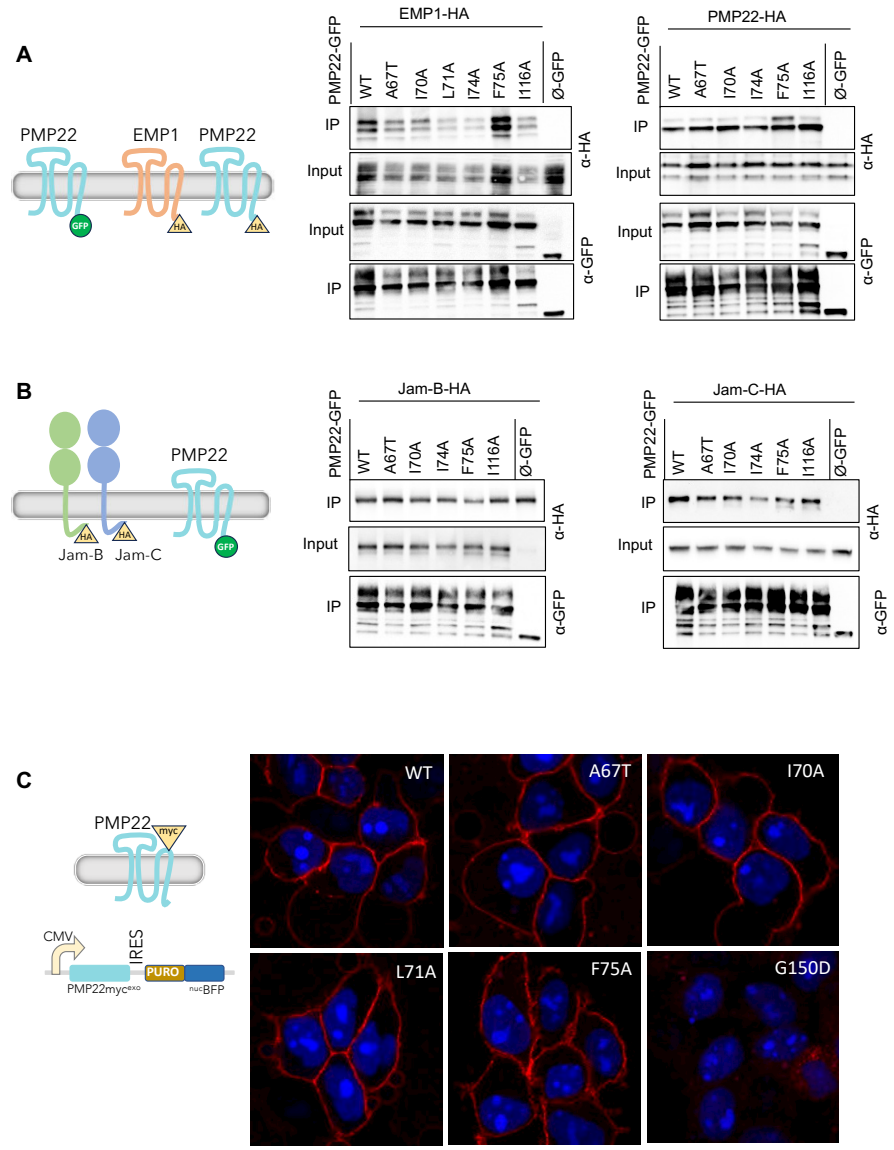

Figure 6. Specificity of PMP22 mutants lacking the ability to bind MPZ.

A. PMP22-GFP, both WT and the indicated mutants along with GFP alone (Ø-GFP), were assessed for their ability to bind EMP1-HA (left) or PMP22-HA (right). Comparable expression levels of the different PMP22 mutants as well as the efficiency was assessed by immunoblotting input lysates and bead immunoprecipitates with α-GFP antibodies.

B. PMP22-GFP, both WT and the indicated mutants, were assessed for the ability to bind Jam-B-HA (left) and Jam-C (right).

C. The cell surface localization of WT and the indicated mutants of PMP22 was assessed in the context of the PMP22-myc^{exo} protein containing an extracellular (exofacial) myc epitope. Expression of PMP22-myc^{exo} was coupled to the expression of a nuclear-localized puromycin-blue fluorescent protein fusion by having it downstream of an internal ribosome entry site on the PMP22 mRNA. Stable transfected HEK293 cell lines expressing these mutants were fixed, left unpermeablized and labelled with α-myc monoclonal antibody and Alexa 568 secondary antibody prior to visualization by confocal microscopy (right).

domains mediate interaction between PMP22 and MPZ. In contrast, our data support the model that PMP22 and MPZ interact in the same membrane bilayer *via* their TMDs and this is both necessary and sufficient for the formation of the complex. This hypothesis is supported by chimeric proteins made of MPZ and its related single Ig-like domain family members whereby proteins with the MPZ TMD were able to interact with PMP22 whereas substitution of the extracellular domain of MPZ with that of SCN2B or MPZL1 had no effect on interaction with PMP22. This model was further verified with point mutations in both MPZ and PMP22 that perturb complex formation and cluster within the TMD of MPZ and the second transmembrane helix of PMP22, respectively. In addition, we find that the PMP22~MPZ complex can be recovered when both are expressed in the same cell, but not when each is expressed in separate cell populations and mixed after cell lysis, and that interaction determined by FRET occurred within plasma membrane segments that were not juxtaposed to other cells. These data further rationalize the model in Figure 5 that the PMP22~MPZ forms in *cis* within the same membrane.

PMP22 plays a crucial role in myelin formation and its homozygous loss results in severe demyelinating neuropathy (Adlkofer et al., 1997; Adlkofer et al., 1995; Chance et al., 1993). Heterozygous loss of *PMP22* results in a more mild peripheral neuropathy, HNPP (Hereditary Neuropathy with Pressure Palsies). We found the A67T patient variant of PMP22 that also causes a partial loss-of-function HNPP-like phenotype also blocks MPZ association but preserves PMP22 trafficking and interactions with other proteins. These data strongly suggest that association of PMP22 with MPZ is a critically important requirement for PMP22 to fulfill its function in myelin. This poses two complementary questions about the molecular and cellular functions of the PMP22~MPZ complex.

One question is what the role of MPZ~PMP22 complex formation is to promote normal myelination. Overall, little is known about what PMP22 does at the molecular level. PMP22 binds cholesterol and can distort lipid bilayers, organize lipid subdomains, coordinate the actin cytoskeleton dynamics, and in some cells coordinate formation of cell-cell tight junctions (Fabbretti et al., 1995; Lee et al., 2014; Marinko et al., 2020b; Notterpek et al., 2001; Vanoye et al., 2019; Zhou et al., 2020; Zhou et al., 2019). PMP22 is also required for proper biogenesis of junctions that maintain the morphology of the paranodal loops of myelin (Guo et al., 2014). MPZ is largely restricted to compact myelin that is enriched in cholesterol and proper levels of cholesterol are required for the trafficking of MPZ to myelin wraps in compact myelin (Poitelon et al., 2020; Saher et al., 2009). One possibility is that PMP22 helps organize lipid subdomains that organize and cluster MPZ to better fulfill its role as an adhesion protein. Alternatively, PMP22 itself might directly perform adhesive activity that amplifies the adhesion properties of MPZ to which it is complexed. There may also be effects on the biogenesis of PMP22 that are helped by association with MPZ. Complex formation could potentially control the levels and distribution of PMP22. A sizable fraction of PMP22 is degraded in Schwann cells rather than sent to the plasma membrane (Pareek et al., 1997). In heterologous cells, a large proportion of PMP22 is trapped in the ER and that proportion increases with increased expression of PMP22 (Marinko et al., 2020a). PMP22 can also be found in aggresomes suggesting that PMP22 is inefficiently exported from the ER and may also be an inefficient substrate for ER-associated degradation (Fortun et al., 2006; Lee et al., 2018). Complex formation with MPZ might potentiate the ability of PMP22 to exit the ER or help control levels of PMP22 by regulating its recognition by the ERAD machinery.

A second question is whether complex formation with MPZ plays a pathogenic role in CMT, especially CMT1A that results from a gene duplication of *PMP22* resulting in disease caused by mild over-expression of wildtype PMP22. One potential mechanism for the pathogenesis of CMT1A may be due to ER-stress from excess production of PMP22 (Bai et al., 2022; Hara et al., 2014; Marinko et al., 2020a; Pantera et al., 2020), that could be exacerbated by alteration of membrane morphology and perturbation of cholesterol distribution (Mittendorf et al., 2017; Zhou et al., 2020; Zhou et al., 2019). These effects would be mediated by simply too much PMP22 in the ER and motivates the therapeutic strategy of reducing PMP22 levels (Boutary et al., 2021). However, CMT1A could be caused not simply by more PMP22 *per se* but rather too much of the PMP22~MPZ complex. Alternatively, the ability of excess PMP22 to form a complex with MPZ may be protective, reducing the severity of CMT that excess PMP22 would otherwise cause if it was unable to form a complex with MPZ. Either of these possibilities would open new therapeutic opportunities to find drugs that could weaken or strengthen the association of PMP22 with MPZ. Now that we have defined mutations in MPZ and PMP22 that specifically block complex formation but preserve other protein interactions and proper trafficking to the cell surface, experiments aimed at understanding the cellular and physiological functions of the PMP22~MPZ complex in vivo and its potential role in driving pathogenesis of CMT1A can now be addressed.

References

Adlkofer, K., R. Frei, D.H. Neuberg, J. Zielasek, K.V. Toyka, and U. Suter. 1997. Heterozygous peripheral myelin protein 22-deficient mice are affected by a progressive demyelinating tomaculous neuropathy. J Neurosci. 17:4662-4671.

Adlkofer, K., R. Martini, A. Aguzzi, J. Zielasek, K.V. Toyka, and U. Suter. 1995. Hypermyelination and demyelinating peripheral neuropathy in Pmp22-deficient mice. Nat Genet. 11:274-280.

Ahmat Amin, M.K.B., A. Shimizu, and H. Ogita. 2019. The Pivotal Roles of the Epithelial Membrane Protein Family in Cancer Invasiveness and Metastasis. Cancers (Basel). 11.

Amici, S.A., W.A. Dunn, Jr., A.J. Murphy, N.C. Adams, N.W. Gale, D.M. Valenzuela, G.D. Yancopoulos, and L. Notterpek. 2006. Peripheral

myelin protein 22 is in complex with alpha6beta4 integrin, and its absence alters the Schwann cell basal lamina. J Neurosci. 26:1179-1189.

Bai, Y., C. Treins, V.G. Volpi, C. Scapin, C. Ferri, R. Mastrangelo, T. Touvier, F. Florio, F. Bianchi, U. Del Carro, F.F. Baas, D. Wang, P. Miniou, P. Guedat, M.E. Shy, and M. D'Antonio. 2022. Treatment with IFB-088 Improves Neuropathy in CMT1A and CMT1B Mice. Mol Neurobiol. 59:4159-4178.

Boutary, S., A. Echaniz-Laguna, D. Adams, J. Loisel-Duwattez, M. Schumacher, C. Massaad, and L. Massaad-Massade. 2021. Treating PMP22 gene duplication-related Charcot-Marie-Tooth disease: the past, the present and the future. Transl Res. 227:100-111.

Castello-Serrano, I., J.H. Lorent, R. Ippolito, K.R. Levental, and I. Levental. 2020. Myelin-Associated MAL and PLP Are Unusual among Multipass Transmembrane Proteins in Preferring Ordered Membrane Domains. J Phys Chem B. 124:5930-5939.

Chance, P.F., M.K. Alderson, K.A. Leppig, M.W. Lensch, N. Matsunami, B. Smith, P.D. Swanson, S.J. Odelberg, C.M. Disteche, and T.D. Bird. 1993. DNA deletion associated with hereditary neuropathy with liability to pressure palsies. Cell. 72:143-151.

Clementel, D., A. Del Conte, A.M. Monzon, G.F. Camagni, G. Minervini, D. Piovesan, and S.C.E. Tosatto. 2022. RING 3.0: fast generation of probabilistic residue interaction networks from structural ensembles. Nucleic Acids Res. 50:W651-W656.

Colby, J., R. Nicholson, K.M. Dickson, W. Orfali, R. Naef, U. Suter, and G.J. Snipes. 2000. PMP22 carrying the trembler or trembler-J mutation is intracellularly retained in myelinating Schwann cells. Neurobiol Dis. 7:561-573.

D'Urso, D., P.J. Brophy, S.M. Staugaitis, C.S. Gillespie, A.B. Frey, J.G. Stempak, and D.R. Colman. 1990. Protein zero of peripheral nerve myelin: biosynthesis, membrane insertion, and evidence for homotypic interaction. Neuron. 4:449-460.

D'Urso, D., P. Ehrhardt, and H.W. Muller. 1999. Peripheral myelin protein 22 and protein zero: a novel association in peripheral nervous system myelin. J Neurosci. 19:3396-3403.

D'Urso, D., R. Prior, R. Greiner-Petter, A.A. Gabreels-Festen, and H.W. Muller. 1998. Overloaded endoplasmic reticulum-Golgi compartments, a possible pathomechanism of peripheral neuropathies caused by mutations of the peripheral myelin protein PMP22. J Neurosci. 18:731-740.

Dickson, K.M., J.J. Bergeron, I. Shames, J. Colby, D.T. Nguyen, E. Chevet, D.Y. Thomas, and G.J. Snipes. 2002. Association of calnexin with mutant peripheral myelin protein-22 ex vivo: a basis for "gain-of-function" ER diseases. Proc Natl Acad Sci U S A. 99:9852-9857.

Ding, S., X. Wu, G. Li, M. Han, Y. Zhuang, and T. Xu. 2005. Efficient transposition of the piggyBac (PB) transposon in mammalian cells and mice. Cell. 122:473-483.

Dominguez, C., R. Boelens, and A.M. Bonvin. 2003. HADDOCK: a protein-protein docking approach based on biochemical or biophysical information. J Am Chem Soc. 125:1731-1737.

Eichberg, J., and S. Iyer. 1996. Phosphorylation of myelin protein: recent advances. Neurochem Res. 21:527-535.

Eylar, E.H., K. Uyemura, S.W. Brostoff, K. Kitamura, A. Ishaque, and S. Greenfield. 1979. Proposed nomenclature for PNS myelin proteins. Neurochem Res. 4:289-293.

Fabbretti, E., P. Edomi, C. Brancolini, and C. Schneider. 1995. Apoptotic phenotype induced by overexpression of wild-type gas3/PMP22: its relation to the demyelinating peripheral neuropathy CMT1A. Genes Dev. 9:1846-1856.

Fantin, S.M., K.F. Parson, P. Yadav, B. Juliano, G.C. Li, C.R. Sanders, M.D. Ohi, and B.T. Ruotolo. 2021. Ion mobility-mass spectrometry reveals the role of peripheral myelin protein dimers in peripheral neuropathy. Proc Natl Acad Sci U S A. 118.

Filbin, M.T., F.S. Walsh, B.D. Trapp, J.A. Pizzey, and G.I. Tennekoon. 1990. Role of myelin P0 protein as a homophilic adhesion molecule. Nature. 344:871-872.

Filbin, M.T., K. Zhang, W. Li, and Y. Gao. 1999. Characterization of the effect on adhesion of different mutations in myelin P0 protein. Ann N Y Acad Sci. 883:160-167.

Fink, A., N. Sal-Man, D. Gerber, and Y. Shai. 2012. Transmembrane domains interactions within the membrane milieu: principles, advances and challenges. Biochim Biophys Acta. 1818:974-983.

Fridman, V., B. Bundy, M.M. Reilly, D. Pareyson, C. Bacon, J. Burns, J. Day, S. Feely, R.S. Finkel, T. Grider, C.A. Kirk, D.N. Herrmann, M. Laura, J. Li, T. Lloyd, C.J. Sumner, F. Muntoni, G. Piscosquito, S. Ramchandren, R. Shy, C.E. Siskind, S.W. Yum, I. Moroni, E. Pagliano, S. Zuchner, S.S. Scherer, M.E. Shy, and C. Inherited Neuropathies. 2015. CMT subtypes and disease burden in patients enrolled in the Inherited Neuropathies Consortium natural history study: a cross-sectional analysis. J Neurol Neurosurg Psychiatry. 86:873-878.

Fridman, V., S. Sillau, J. Bockhorst, K. Smith, I. Moroni, E. Pagliano, C. Pisciotta, G. Piscosquito, M. Laura, F. Muntoni, C. Bacon, S. Feely, T. Grider, L. Gutmann, R. Shy, J. Wilcox, D.N. Herrmann, J. Li, S. Ramchandren, C.J. Sumner, T.E. Lloyd, J. Day, C.E. Siskind, S.W. Yum, R. Sadjadi, R.S. Finkel, S.S. Scherer, D. Pareyson, M.M. Reilly, M.E. Shy, and N. Inherited Neuropathies Consortium-Rare Diseases Clinical Research. 2023. Disease Progression in Charcot-Marie-Tooth Disease Related to MPZ Mutations: A Longitudinal Study. Ann Neurol. 93:563-576.

Giese, K.P., R. Martini, G. Lemke, P. Soriano, and M. Schachner. 1992. Mouse P0 gene disruption leads to hypomyelination, abnormal expression of recognition molecules, and degeneration of myelin and axons. Cell. 71:565-576.

Greenfield, S., S. Brostoff, E.H. Eylar, and P. Morell. 1973. Protein composition of myelin of the peripheral nervous system. J Neurochem. 20:1207-1216.

Guo, J., L. Wang, Y. Zhang, J. Wu, S. Arpag, B. Hu, B.A. Imhof, X. Tian, B.D. Carter, U. Suter, and J. Li. 2014. Abnormal junctions and permeability of myelin in PMP22-deficient nerves. Ann Neurol. 75:255-265.

Hara, T., Y. Hashimoto, T. Akuzawa, R. Hirai, H. Kobayashi, and K. Sato. 2014. Rer1 and calnexin regulate endoplasmic reticulum retention of a peripheral myelin protein 22 mutant that causes type 1A Charcot-Marie-Tooth disease. Sci Rep. 4:6992.

Hasse, B., F. Bosse, H. Hanenberg, and H.W. Muller. 2004. Peripheral myelin protein 22 kDa and protein zero: domain specific trans-interactions. Mol Cell Neurosci. 27:370-378.

Hasse, B., F. Bosse, and H.W. Muller. 2002. Proteins of peripheral myelin are associated with glycosphingolipid/cholesterol-enriched membranes. J Neurosci Res. 69:227-232.

Hayasaka, K., A. Ohnishi, G. Takada, Y. Fukushima, and Y. Murai. 1993. Mutation of the myelin P0 gene in Charcot-Marie-tooth neuropathy type 1. Biochem Biophys Res Commun. 194:1317-1322.

Jetten, A.M., and U. Suter. 2000. The peripheral myelin protein 22 and epithelial membrane protein family. Prog Nucleic Acid Res Mol Biol. 64:97-129.

Jumper, J., R. Evans, A. Pritzel, T. Green, M. Figurnov, O. Ronneberger, K. Tunyasuvunakool, R. Bates, A. Zidek, A. Potapenko, A. Bridgland, C. Meyer, S.A.A. Kohl, A.J. Ballard, A. Cowie, B. Romera-Paredes, S. Nikolov, R. Jain, J. Adler, T. Back, S. Petersen, D. Reiman, E. Clancy, M. Zielinski, M. Steinegger, M. Pacholska, T. Berghammer, S. Bodenstein, D. Silver, O. Vinyals, A.W. Senior, K. Kavukcuoglu, P. Kohli, and D.

Hassabis. 2021. Highly accurate protein structure prediction with AlphaFold. Nature. 596:583-+.

Jung, J., H. Coe, and M. Michalak. 2011. Specialization of endoplasmic reticulum chaperones for the folding and function of myelin glycoproteins P0 and PMP22. FASEB J. 25:3929-3937.

Lee, S., S. Amici, H. Tavori, W.M. Zeng, S. Freeland, S. Fazio, and L. Notterpek. 2014. PMP22 is critical for actin-mediated cellular functions and for establishing lipid rafts. J Neurosci. 34:16140-16152.

Lee, S., H. Bazick, V. Chittoor-Vinod, M.O. Al Salihi, G. Xia, and L. Notterpek. 2018. Elevated Peripheral Myelin Protein 22, Reduced Mitotic Potential, and Proteasome Impairment in Dermal Fibroblasts from Charcot-Marie-Tooth Disease Type 1A Patients. Am J Pathol. 188:728-738.

Lemke, G., and R. Axel. 1985. Isolation and sequence of a cDNA encoding the major structural protein of peripheral myelin. Cell. 40:501-508.

Li, J., B. Parker, C. Martyn, C. Natarajan, and J. Guo. 2013. The PMP22 gene and its related diseases. Mol Neurobiol. 47:673-698.

Liu, N., J. Yamauchi, and E.M. Shooter. 2004. Recessive, but not dominant, mutations in peripheral myelin protein 22 gene show unique patterns of aggregation and intracellular trafficking. Neurobiol Dis. 17:300-309.

Lomize, M.A., I.D. Pogozheva, H. Joo, H.I. Mosberg, and A.L. Lomize. 2012. OPM database and PPM web server: resources for positioning of proteins in membranes. Nucleic Acids Res. 40:D370-376.

Lupski, J.R., C.A. Wise, A. Kuwano, L. Pentao, J.T. Parke, D.G. Glaze, D.H. Ledbetter, F. Greenberg, and P.I. Patel. 1992. Gene dosage is a mechanism for Charcot-Marie-Tooth disease type 1A. Nat Genet. 1:29-33.

Mandich, P., G.L. Mancardi, A. Varese, S. Soriani, E. Di Maria, E. Bellone, M. Bado, L. Gross, A.J. Windebank, F. Ajmar, and A. Schenone. 1999. Congenital hypomyelination due to myelin protein zero Q215X mutation. Ann Neurol. 45:676-678.

Marinko, J.T., B.D. Carter, and C.R. Sanders. 2020a. Direct relationship between increased expression and mistrafficking of the Charcot-Marie-Tooth-associated protein PMP22. J Biol Chem. 295:11963-11970.

Marinko, J.T., A.K. Kenworthy, and C.R. Sanders. 2020b. Peripheral myelin protein 22 preferentially partitions into ordered phase membrane domains. Proc Natl Acad Sci U S A. 117:14168-14177.

Marinko, J.T., M.T. Wright, J.P. Schlebach, K.R. Clowes, D.R. Heintzman, L. Plate, and C.R. Sanders. 2021. Glycosylation limits forward trafficking of the tetraspan membrane protein PMP22. J Biol Chem. 296:100719.

Meng, E.C., E.F. Pettersen, G.S. Couch, C.C. Huang, and T.E. Ferrin. 2006. Tools for integrated sequence-structure analysis with UCSF Chimera. BMC Bioinformatics. 7:339.

Mittendorf, K.F., B.M. Kroncke, J. Meiler, and C.R. Sanders. 2014. The homology model of PMP22 suggests mutations resulting in peripheral neuropathy disrupt transmembrane helix packing. Biochemistry. 53:6139-6141.

Mittendorf, K.F., J.T. Marinko, C.M. Hampton, Z. Ke, A. Hadziselimovic, J.P. Schlebach, C.L. Law, J. Li, E.R. Wright, C.R. Sanders, and M.D. Ohi. 2017. Peripheral myelin protein 22 alters membrane architecture. Sci Adv. 3:e1700220.

Molinarolo, S., D. Granata, V. Carnevale, and C.A. Ahern. 2018. Mining Protein Evolution for Insights into Mechanisms of Voltage-Dependent Sodium Channel Auxiliary Subunits. Handb Exp Pharmacol. 246:33-49.

Murphy, S.M., M. Laura, K. Fawcett, A. Pandraud, Y.T. Liu, G.L. Davidson, A.M. Rossor, J.M. Polke, V. Castleman, H. Manji, M.P. Lunn, K. Bull, G. Ramdharry, M. Davis, J.C. Blake, H. Houlden, and M.M. Reilly. 2012. Charcot-Marie-Tooth disease: frequency of genetic subtypes and guidelines for genetic testing. J Neurol Neurosurg Psychiatry. 83:706-710.

Nodera, H., M. Nishimura, E.L. Logigian, D.N. Herrmann, and R. Kaji. 2003. HNPP due to a novel missense mutation of the PMP22 gene. Neurology. 60:1863-1864.

Notterpek, L., K.J. Roux, S.A. Amici, A. Yazdanpour, C. Rahner, and B.S. Fletcher. 2001. Peripheral myelin protein 22 is a constituent of intercellular junctions in epithelia. Proc Natl Acad Sci U S A. 98:14404-14409.

Pantera, H., M.E. Shy, and J. Svaren. 2020. Regulating PMP22 expression as a dosage sensitive neuropathy gene. Brain Res. 1726:146491.

Pareek, S., L. Notterpek, G.J. Snipes, R. Naef, W. Sossin, J. Laliberte, S. Iacampo, U. Suter, E.M. Shooter, and R.A. Murphy. 1997. Neurons promote the translocation of peripheral myelin protein 22 into myelin. J Neurosci. 17:7754-7762.

Poitelon, Y., A.M. Kopec, and S. Belin. 2020. Myelin Fat Facts: An Overview of Lipids and Fatty Acid Metabolism. Cells. 9.

Ptak, C.P., T.A. Peterson, J.B. Hopkins, C.A. Ahern, M.E. Shy, and R.C. Piper. 2023. Homomeric interactions of the MPZ Ig domain and their relation to Charcot-Marie-Tooth disease. Brain. 146:5110-5123.

Qin, Y., S. Mohandessi, L. Gordon, and M. Wadehra. 2015. Regulation of FAK Activity by Tetraspan Proteins: Potential Clinical Implications in Cancer. Crit Rev Oncog. 20:391-405.

Rao, R.G., D. Sudhakar, C.P. Hogue, S. Amici, L.K. Gordon, J. Braun, L. Notterpek, L. Goodglick, and M. Wadehra. 2011. Peripheral myelin protein-22 (PMP22) modulates alpha 6 integrin expression in the human endometrium. Reprod Biol Endocrinol. 9:56.

Rossor, A.M., J.M. Polke, H. Houlden, and M.M. Reilly. 2013. Clinical implications of genetic advances in Charcot-Marie-Tooth disease. Nat Rev Neurol. 9:562-571.

Roux, K.J., S.A. Amici, B.S. Fletcher, and L. Notterpek. 2005. Modulation of epithelial morphology, monolayer permeability, and cell migration by growth arrest specific 3/peripheral myelin protein 22. Mol Biol Cell. 16:1142-1151.

Saher, G., S. Quintes, W. Mobius, M.C. Wehr, E.M. Kramer-Albers, B. Brugger, and K.A. Nave. 2009. Cholesterol regulates the endoplasmic reticulum exit of the major membrane protein P0 required for peripheral myelin compaction. J Neurosci. 29:6094-6104.

Sakakura, M., A. Hadziselimovic, Z. Wang, K.L. Schey, and C.R. Sanders. 2011. Structural basis for the Trembler-J phenotype of Charcot-Marie-Tooth disease. Structure. 19:1160-1169.

Sakakura, M., M. Tanabe, M. Mori, H. Takahashi, and K. Mio. 2023. Structural bases for the Charcot-Marie-Tooth disease induced by single amino acid substitutions of myelin protein zero. Structure.

Schlebach, J.P., M. Narayan, C. Alford, K.F. Mittendorf, B.D. Carter, J. Li, and C.R. Sanders. 2015. Conformational Stability and Pathogenic Misfolding of the Integral Membrane Protein PMP22. J Am Chem Soc. 137:8758-8768.

Schlebach, J.P., D. Peng, B.M. Kroncke, K.F. Mittendorf, M. Narayan, B.D. Carter, and C.R. Sanders. 2013. Reversible folding of human peripheral

myelin protein 22, a tetraspan membrane protein. Biochemistry. 52:3229-3241.

Shapiro, L., J.P. Doyle, P. Hensley, D.R. Colman, and W.A. Hendrickson. 1996. Crystal structure of the extracellular domain from P0, the major structural protein of peripheral nerve myelin. Neuron. 17:435-449.

Simske, J.S. 2013. Claudins reign: The claudin/EMP/PMP22/gamma channel protein family in C. elegans. Tissue Barriers. 1:e25502.

Skre, H. 1974. Genetic and clinical aspects of Charcot-Marie-Tooth's disease. Clin Genet. 6:98-118.

Suzuki, H., T. Nishizawa, K. Tani, Y. Yamazaki, A. Tamura, R. Ishitani, N. Dohmae, S. Tsukita, O. Nureki, and Y. Fujiyoshi. 2014. Crystal structure of a claudin provides insight into the architecture of tight junctions. Science. 344:304-307.

Timmerman, V., E. Nelis, W. Van Hul, B.W. Nieuwenhuijsen, K.L. Chen, S. Wang, K. Ben Othman, B. Cullen, R.J. Leach, C.O. Hanemann, and et al. 1992. The peripheral myelin protein gene PMP-22 is contained within the Charcot-Marie-Tooth disease type 1A duplication. Nat Genet. 1:171-175.

Tobler, A.R., N. Liu, L. Mueller, and E.M. Shooter. 2002. Differential aggregation of the Trembler and Trembler J mutants of peripheral myelin protein 22. Proc Natl Acad Sci U S A. 99:483-488.

Tobler, A.R., L. Notterpek, R. Naef, V. Taylor, U. Suter, and E.M. Shooter. 1999. Transport of Trembler-J mutant peripheral myelin protein 22 is blocked in the intermediate compartment and affects the transport of the wild-type protein by direct interaction. J Neurosci. 19:2027-2036.

Tramier, M., M. Zahid, J.C. Mevel, M.J. Masse, and M. Coppey-Moisan. 2006. Sensitivity of CFP/YFP and GFP/mCherry pairs to donor photobleaching on FRET determination by fluorescence lifetime imaging microscopy in living cells. Microsc Res Tech. 69:933-939.

Uyemura, K., H. Asou, and Y. Takeda. 1995. Structure and function of peripheral nerve myelin proteins. Prog Brain Res. 105:311-318.

Valbuena, F.M., I. Fitzgerald, R.L. Strack, N. Andruska, L. Smith, and B.S. Glick. 2020. A photostable monomeric superfolder green fluorescent protein. Traffic. 21:534-544.

Van Itallie, C.M., and J.M. Anderson. 2006. Claudins and epithelial paracellular transport. Annu Rev Physiol. 68:403-429.

van Paassen, B.W., A.J. van der Kooi, K.Y. van Spaendonck-Zwarts, C. Verhamme, F. Baas, and M. de Visser. 2014. PMP22 related neuropathies: Charcot-Marie-Tooth disease type 1A and Hereditary Neuropathy with liability to Pressure Palsies. Orphanet J Rare Dis. 9:38.

van Zundert, G.C.P., J. Rodrigues, M. Trellet, C. Schmitz, P.L. Kastritis, E. Karaca, A.S.J. Melquiond, M. van Dijk, S.J. de Vries, and A. Bonvin. 2016. The HADDOCK2.2 Web Server: User-Friendly Integrative Modeling of Biomolecular Complexes. J Mol Biol. 428:720-725.

Vanoye, C.G., M. Sakakura, R.M. Follis, A.J. Trevisan, M. Narayan, J. Li, C.R. Sanders, and B.D. Carter. 2019. Peripheral myelin protein 22 modulates store-operated calcium channel activity, providing insights into Charcot-Marie-Tooth disease etiology. J Biol Chem. 294:12054-12065.

Wu, E.L., X. Cheng, S. Jo, H. Rui, K.C. Song, E.M. Davila-Contreras, Y. Qi, J. Lee, V. Monje-Galvan, R.M. Venable, J.B. Klauda, and W. Im. 2014. CHARMM-GUI Membrane Builder toward realistic biological membrane simulations. J Comput Chem. 35:1997-2004.

Xu, W., M. Shy, J. Kamholz, L. Elferink, G. Xu, J. Lilien, and J. Balsamo. 2001. Mutations in the cytoplasmic domain of P0 reveal a role for PKC-mediated phosphorylation in adhesion and myelination. J Cell Biol. 155:439-446.

Zhou, Y., D. Borchelt, J.C. Bauson, S. Fazio, J.R. Miles, H. Tavori, and L. Notterpek. 2020. Subcellular diversion of cholesterol by gain- and loss-of-function mutations in PMP22. Glia. 68:2300-2315.

Zhou, Y., J.R. Miles, H. Tavori, M. Lin, H. Khoshbouei, D.R. Borchelt, H. Bazick, G.E. Landreth, S. Lee, S. Fazio, and L. Notterpek. 2019. PMP22 Regulates Cholesterol Trafficking and ABCA1-Mediated Cholesterol Efflux. J Neurosci. 39:5404-5418.

Zoidl, G., S. Blass-Kampmann, D. D'Urso, C. Schmalenbach, and H.W. Muller. 1995. Retroviral-mediated gene transfer of the peripheral myelin protein PMP22 in Schwann cells: modulation of cell growth. EMBO J. 14:1122-1128.

Acknowledgements

We acknowledge the University of Iowa personnel and instrumentation in the IIHG Genomic Sequencing, the Carver College of Medicine NMR, and Protein & Crystallography core facilities, supported by the Roy J. and Lucille A. Carver College of Medicine and grants from the Roy J. Carver Charitable Trust. We thank Miranda Schene and Sandipan Chowdhury for help with detergent and FPLC analysis. This work was supported by NIH-R01 R35GM148239 to CAA, U54NS065712 to MES, and NIH RO1GM058202 to RCP. CAA and RCP were supported by the Roy J. Carver Charitable Trust. This paper was typeset with the bioRxiv word template by @Chrelli: www.github.com/chrelli/bioRxiv-word-template

Competing interest statement

The authors have no competing interests to declare.

Materials and Methods

Plasmids, antibodies, cell culture, and materials

Gene synthesized open reading frames were purchased from IDT (Coralville, IA), subcloned into expression plasmids by Gibson assembly (e.g. pcDNA3.1, ThermoFisher, Waltham, MA), and sequenced by Sanger sequencing and/or Oxford nanopore long-read technology using Plasmidsaurus (Eugene, OR). Plasmid use and description are provided in *Supplementary Table 1* and the full sequence of plasmids provided in additional supplementary materials. GFP tagging of MPZ, PMP22, and Glycophorin A was done using msGFP2 (Valbuena et al., 2020), a monomeric superfolder version of GFP that was stable against photobleaching. Antibodies used were: mouse α-GFP monoclonal (sc-9996, Santa Cruz Technology, Santa Cruz, CA), mouse α-HA monoclonal (901514, BioLegend, San Diego, CA), mouse α-myc-Tag (9B11) monoclonal (2276, Cell Signaling Technology, Danvers, MA), rabbit α-mCherry polyclonal (AB356482, EMD Millipore Corp., Burlington, MA). Peroxidase-conjugated (HRP) α-mouse (cat#:70776S) or α-rabbit secondary antibody (cat# 7074S) were obtained from Cell Signaling Technology. Dodecyl-β-D-maltoside (DDM) and cholesteryl hemisuccinate (CHS) from Anatrace (Maumee, OH) were kept as a stock solution (10% and 2%, respectively) in 200mM Tris pH 8.0 at 4°C. Protease inhibitors cOmplete lacking EDTA, and Pefabloc, were obtained from Sigma (St. Louis, MO).

HEK293 cells (ATCC: CRL-1573) and RT4-D6P2T Schwannoma cells (ATCC: CRL-2768) were cultured at 37°C with 5% CO2 in Dulbecco's modified Eagle's medium (DMEM) supplemented with 10% fetal bovine serum (FBS) and 1% penicillin + streptomycin antibiotics (Gibco, Grand Island, NY). Transient transfections were accomplished with Lipofectamine LTX using 5 μg plasmid DNA per million cells in Opti-MEM reduced serum media according to manufacturer's instruction (ThermoFisher, Waltham, MA). After transfection, cells were cultured in DMEM with 10% FBS without antibiotics prior to analysis. Stable transfected PMP22-myc^{exo} cell lines were made using the piggyBac system (Ding et al., 2005) and a co-expression vector with the puromycin-resistance protein fused to blue fluorescent protein (mTAGBFP2) appended with a nuclear localization signal. At 24 hrs post transfection, cells were grown in DMEM media with 10% FBS and 5 μg/ml puromycin (Sigma, St. Louis, MO). Cells expressing mTAGBFP2 were sorted from non-mTAGBFP2 expressing cells by flow cytometry.

Immunoprecipitation

Anti-GFP nanobody-conjugated agarose beads (Protein Crystallograpy facility, University of Iowa) were used for immunoprecipitations. Cells were grown in 6 cm dishes, 18-20 hrs post transfection washed with Dulbecco's phosphate-buffered saline (DPBS) and suspended with Versene (ThermoFisher, Waltham, MA). Cells were lysed for 30 min on ice in 500 μl lysis buffer (PBS with 1% DDM, 0.2% CHS, supplemented with cOmpleteTM, and Pefabloc® protease inhibitors) and centrifuged at 4°C 12,200 rpm for 15 min. The cleared supernatant (400 μl) was mixed with 34 μl of α-GFP nanobody agarose beads in 100 μl PBS and incubated 1 hr rotating at 4°C. After three washes by centrifugation at 5,000 rpm 4 min with 1ml of cold lysis buffer diluted 8 times with PBS, proteins were eluted with SDS-loading

sample buffer with heating at 95°C. Equal amounts of whole cell lysates (input) and immunoprecipitated proteins were resolved by SDS-PAGE then immunoblotted with indicated antibodies.

Fluorescence microscopy

HEK293 cells were grown on glass bottom dishes (MatTek, P35G-1.5-20-C). After 18-20 hrs of transfection, live cells expressing either GFP and/or mCherry tagged proteins were visualized in the culture media using a Leica SP8 confocal microscope equipped with 405, 488 and 552 nm lasers.

For FRET analysis, cells were fixed in 4% paraformaldehyde in DPBS, washed with 50 mM Tris-HCl in DPBS pH7.5 to inactivate residual fixative, and imaged in DPBS. The Leica LAX X Microlab software was used using the FRET AB acceptor photobleaching method with the msGFP/mCherry pair of fluorophores (Tramier et al., 2006). For visualization of stable cell lines with wild type or mutant PMP22-myc^{exo} at the cell surface, cells were grown on glass coverslips in 6-well culture plates, fixed with 4% paraformaldehyde in DPBS 15 min, washed with 50 mM Tris-HCl in DPBS pH 7.5, then washed with DPBS. Coverslips were blocked with 5% goat serum in DPBS for 30 min, then incubated with mouse α-myc-tag antibody 40 min at RT. Following three washes with DPBS, coverslips were incubated with goat α-mouse Alexa568 secondary antibody for 30 min in the dark. Following three washes with DPBS, the coverslips were mounted on glass slides using Vectashield antifade mounting medium (H-1000, Vector Laboratories, Burlingame, CA).

Modeling

Models for PMP22 (AF-Q01453-F1) and MPZ (AF-P25189-F1) were obtained from the AlphaFold PSDB (Jumper et al., 2021). The complex between PMP22 (all residues) and MPZ (transmembrane residues: R153-L184) was modelled using the HADDOCK webserver (Dominguez et al., 2003; van Zundert et al., 2016) with initial restraints defined by all residues shown to disrupt the complex when experimentally mutated (on PMP22: A67, I70, I71, I73, I74, F75, I116; on MPZ: G155, V157, L158, I162, L166, V169). The best models from the two top ranking MPZ docking poses exhibited mutually exclusive interactions with restraints and were each further refined on a subset of residue restraints (*Supplemental Figure 1*). The final model that best rationalizes the mutagenesis data was constrained for involvement of I70 without a requirement for proximity of I116. Full-length MPZ (residues I30-K248) was superimposed (Meng et al., 2006) on the final model and embedded in a representative lipid bilayer (60%POPC:40%cholesterol) using the CHARMM-GUI webserver (Wu et al., 2014) with membrane orientation optimized by the PPM method (Lomize et al., 2012).

Supplementary Table 1. Plasmids Used. The Description of the plasmids and the figures they were used for are described.

plasmid name	description	antibiotic	Map	Figures used
pPL7428	PMP22-msGFP in pcDNA3	Amp	pPL7428	Figure 1A, 1B, 1C, 1E, 2A, 2B, 3A, 3B, 4A, 4B, 5B, 6A, 6B, Suppl.Fig.1
pPL6981	MPZ-HA in pcDNA3	Kanr	pPL6981	Figure 1A,1B,1C,2A,2B
pPL7683	MPZ-HA in pcDNA3	Amp	pPL7683	Figure 3B,4A,4B,5B
pPL7638	MPZ-msGFP2 in pcDNA3	Amp	pPL7638	Figure1B，1D，3B，
pPL7471	EMP3-msGFP in pcDNA3	Amp	pPL7471	Figure1B，2A，2B，4A，6A
pPL7472	PMP22-myc-exo in pcDNA3	Amp	pPL7472	Figure 1D
pPL7549	MPZ-mCherry in pcDNA3	Amp	pPL7549	Figure 1E,3A,3C,
pPL7462	MPZL1-HA in pcDNA3	Amp	pPL7462	Figure 2A, 2B
pPL7463	MPZL2-HA in pcDNA3	Amp	pPL7463	Figure 2A
pPL7466	SCN2B-HA in pcDNA3	Amp	pPL7466	Figure 2A,2B
pPL7467	SCN3B-HA in pcDNA3	Amp	pPL7467	Figure 2A
pPL7468	SCN4B-HA in pcDNA3	Amp	pPL7468	Figure 2A
pPL7579	MPZ/SCN2B-HA chimera A in pcDNA	Amp	pPL7579	Figure 2B
pPL7580	MPZ/SCN2B-HA chimera B in pcDNA	Amp	pPL7580	Figure 2B
pPL7581	MPZ/MPZL1-HA chimera G in pcDNA	Amp	pPL7581	Figure 2B
pPL7582	MPZ/MPZL1-HA chimera H in pcDNA	Amp	pPL7582	Figure 2B
pPL7553	MPZ/SCN2B-HA chimera C in pcDNA	Amp	pPL7553	Figure 2B
pPL7536	MPZ/SCN2B-HA chimera D in pcDNA	Amp	pPL7536	Figure 2B
pPL7537	MPZ/MPZL1-HA chimera E in pcDNA	Amp	pPL7537	Figure 2B
pPL7538	MPZ/MPZL1-HA chimera F in pcDNA	Amp	pPL7538	Figure 2B
pPL7555	R98W_MPZ-mCherry	Amp	made in pPL7549	Figure 3C
pPL7654	G155V_MPZ-mCherry	Amp	made in pPL7549	Figure 3A,3C, Suppl.Fig.3
pPL7714	L158A,G159V_MPZ-mCherry	Amp	made in pPL7549	Figure 3A
pPL7715	I162A,G163V_MPZ-mCherry	Amp	made in pPL7549	Figure 3A
pPL7716	L166A_MPZ-mCherry	Amp	made in pPL7549	Figure 3A
pPL7717	L170A_MPZ-mCherry	Amp	made in pPL7549	Figure 3A
pPL7718	L174A_MPZ-mCherry	Amp	made in pPL7549	Figure 3A
pPL7719	Y177A_MPZ-mCherry	Amp	made in pPL7549	Figure 3A
pPL7720	Y154A_MPZ-mCherry	Amp	made in pPL7549	Figure 3A
pPL7721	A160L_MPZ-mCherry	Amp	made in pPL7549	Figure 3A
pPL7722	G164V_MPZ-mCherry	Amp	made in pPL7549	Figure 3A
pPL7723	G167V_MPZ-mCherry	Amp	made in pPL7549	Figure 3A
pPL7724	L171A_MPZ-mCherry	Amp	made in pPL7549	Figure 3A
pPL7725	L175A_MPZ-mCherry	Amp	made in pPL7549	Figure 3A
pPL7726	V157L_MPZ-mCherry	Amp	made in pPL7549	Figure 3A
pPL7727	V161L_MPZ-mCherry	Amp	made in pPL7549	Figure 3A
pPL7728	L172A, L173A_MPZ-mCherry	Amp	made in pPL7549	Figure 3A
pPL7729	F176A_MPZ-mCherry	Amp	made in pPL7549	Figure 3A
pPL7792	I162A_MPZ-mCherry	Amp	made in pPL7549	Figure 3A,3C, Suppl.Fig.3
pPL7793	G163V_MPZ-mCherry	Amp	made in pPL7549	Figure 3A
pPL7794	G159V_MPZ-mCherry	Amp	made in pPL7549	Figure 3A
pPL7795	I162A,L166A_MPZ-mCherry	Amp	made in pPL7549	Figure 3A
pPL7796	V169L_MPZ-mCherry	Amp	made in pPL7549	Figure 3A
pPL7797	V157A_MPZ-mCherry	Amp	made in pPL7549	Figure 3A
pPL7801	L158A_MPZ-mCherry	Amp	made in pPL7549	Figure 3A,3C, Suppl.Fig.3
pPL7827	G155V,I162A_MPZ-mCherry	Amp	made in pPL7549	Figure 3A,3C, Suppl.Fig.3
pPL7828	G155V,L158A_MPZ-mCherry	Amp	made in pPL7549	Figure 3A,3C, Suppl.Fig.3
pPL7695	G155V_MPZ-HA	Amp	made in pPL7683	Figure 3B
pPL7898	L158A_MPZ-HA	Amp	made in pPL7683	Figure 3B
pPL7899	I162A_MPZ-HA	Amp	made in pPL7683	Figure 3B
pPL7900	G155V,L158A_MPZ-HA	Amp	made in pPL7683	Figure 3B
pPl7901	G155V,I162A_MPZ-HA	Amp	made in pPL7683	Figure 3B
pPL7613	eGFP in pcDNA3	Amp	pPL7613	Figure 2B, 3B, 4A, 6A, 6B
pPL7642	A67T_PMP22-msGFP	Amp	made in pPL7428	Figure 4B, 5B, 6A, 6B
pPL7802	V10L_PMP22-msGFP	Amp	made in pPL7428	Figure 4B
pPL7803	V13L_PMP22-msGFP	Amp	made in pPL7428	Figure 4B
pPL7804	A14I_PMP22-msGFP	Amp	made in pPL7428	Figure 4B
pPL7805	V17I_PMP22-msGFP	Amp	made in pPL7428	Figure 4B
pPL7806	V21A_PMP22-msGFP	Amp	made in pPL7428	Figure 4B
pPL7807	I70A_PMP22-msGFP	Amp	made in pPL7428	Figure 4B, 6A, 6B
pPL7808	I73A_PMP22-msGFP	Amp	made in pPL7428	Figure 4B
pPL7809	I74A_PMP22-msGFP	Amp	made in pPL7428	Figure 4B, 6A, 6B
pPL7810	F75A_PMP22-msGFP	Amp	made in pPL7428	Figure 4B, 6A, 6B
pPL7811	L78A_PMP22-msGFP	Amp	made in pPL7428	Figure 4B
pPL7812	I98A_PMP22-msGFP	Amp	made in pPL7428	Figure 4B
pPL7813	L108A_PMP22-msGFP	Amp	made in pPL7428	Figure 4B
pPL7814	S112A_PMP22-msGFP	Amp	made in pPL7428	Figure 4B
pPL7815	A115L_PMP22-msGFP	Amp	made in pPL7428	Figure 4B
pPL7816	I166A_PMP22-msGFP	Amp	made in pPL7428	Figure 4B, 6A, 6B
pPL7817	I137A_PMP22-msGFP	Amp	made in pPL7428	Figure 4B
pPL7818	V141A_PMP22-msGFP	Amp	made in pPL7428	Figure 4B
pPL7837	L71A_PMP22-msGFP	Amp	made in pPL7428	Figure 4B, 6A, 6B
pPL7741	A115V_PMP22-msGFP	Amp	made in pPL7428	Figure 5B
pPL7742	T118M_PMP22-msGFP	Amp	made in pPL7428	Figure 5B
pPL7743	I137V_PMP22-msGFP	Amp	made in pPL7428	Figure 5B
pPL7469	EMP1-msGFP in pcDNA	Amp	pPL7469	Figure 4A
pPL7470	EMP2-msGFP in pcDNA	Amp	pPL7470	Figure 4A
pPL7628	JAM_B-HA in pcDNA	Amp	pPL7628	Figure 6B
pPL7629	JAM_C-HA in pcDNA	Amp	pPL7629	Figure 6B
pPL7896	EMP1-HA in pcDNA	Amp	pPL7896	Figure 6A
pPL7677	PMP22-HA in pcDNA	Amp	pPL7677	Figure 6A
pPL7881	PMP22_mycEXO in IRES_PacBlue_PB	Amp	pPL7881	Figure 6C, Suppl.Fig 4
pPL7886	G150D_PMP22_mycEXO in IRES_PacBlue_PB	Amp	pPL7886	Figure 6C, Suppl.Fig 4
pPL7885	L71A_PMP22_mycEXO in IRES_PacBlue_PB	Amp	pPL7885	Figure 6C
pPL7883	A67T_PMP22_mycEXO in IRES_PacBlue_PB	Amp	pPL7883	Figure 6C, Suppl.Fig 4
pPL7882	F75A_PMP22_mycEXO in IRES_PacBlue_PB	Amp	pPL7882	Figure 6C
pPL7884	I70A_PMP22_mycEXO in IRES_PacBlue_PB	Amp	pPL7884	Figure 6C

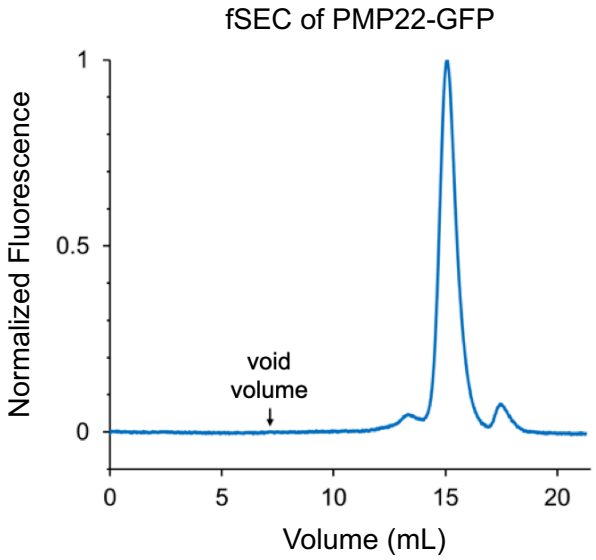

Supplemental Figure 1. Size exclusion chromatography of PMP22-GFP. The solubilized lysate from HEK293 cells expressing GFP-tagged PMP22 was run on an HPLC (Shimadzu) at 0.5 mL/min in PBS buffer containing 0.5% DDM and 0.1% CHS, separated using a Superose 6 10/300 column, and observed by fluorescence detection of the GFP-fusion protein.

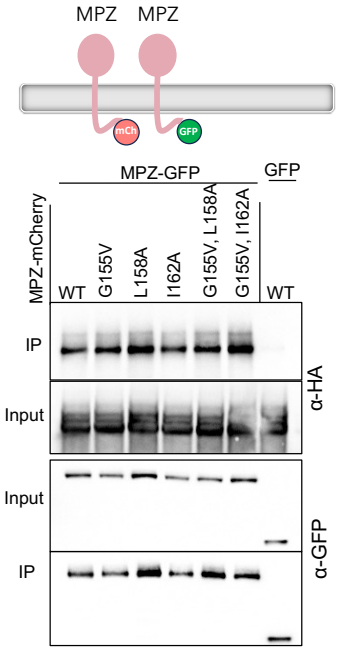

Supplemental Figure 2. **Association of MPZ-mCherry mutants with MPZ-GFP**

WT and the indicated MPZ-mCherry mutants were assessed for their ability to co-immunoprecipitate with MPZ-GFP using α-GFP nanobody beads. Starting input lysate and immunoprecipitates were immunoblotted with α-mCherry and α-GFP antibodies.

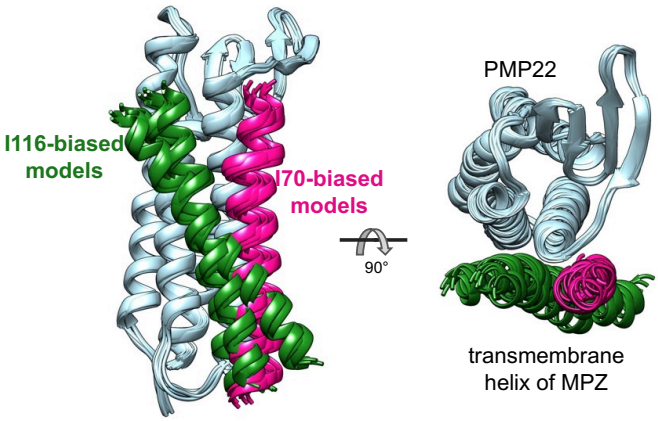

Haddock Residue Restraints	I70-biased models	I116-biased models
PMP22 A67	**active**	passive
PMP22 I70	passive	
PMP22 I71	**active**	**active**
PMP22 I73		
PMP22 I74	passive	
PMP22 F75	**active**	**active**
PMP22 I116		**active**
MPZ G155	passive	
MPZ V157		
MPZ L158	**active**	**active**
MPZ I162	**active**	**active**
MPZ L166	**active**	**active**
MPZ V169	**active**	**active**

Supplementary Figure 3. **Interaction models of the complex between PMP22 and MPZ.** HADDOCK was used to generate a constraint-driven model for the complex between PMP22 (AF-Q01453-F1) and the transmembrane segment of MPZ (AF-P25189-F1). After an initial round of modeling with the full set of HADDOCK residue restraints (listed in table), the resulting feasible poses of model clusters could interact with either I70 or I116 but not both. To limit violations from residues indirectly disrupting the interface, the interaction models were further refined in HADDOCK with the removal of restraints that were irrelevant to the interface for I70- or I116-biased poses. The top 4 models from the one I70-biased model cluster and the two I116-biased model clusters are superimposed on their PMP22 structure (light blue) and depicted with the relative position of the MPZ transmembrane segment (I70-biased – deep pink; I116-biased – forest green). Residue restraints used for the refined HADDOCK docking calculation of biased poses are listed in the table.

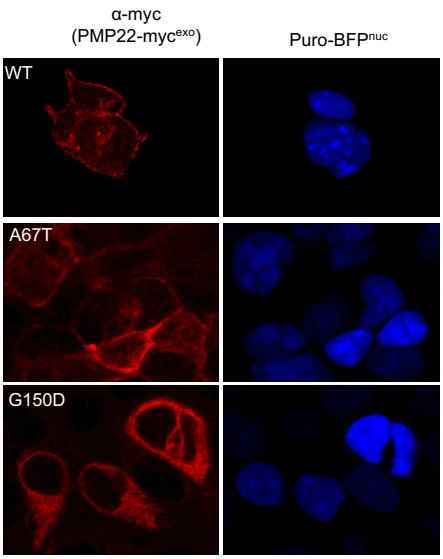

Supplemental Figure 4. **Immunofluorescence Localization of PMP22myc^{exo} mutants in permeabilized cells.**
Cell populations as described in Figure 6C were fixed and immunolabelled as in Figure 6C but with the addition of 0.2% Triton X-100 after fixation to permeabilize cells.